American Mineralogist, Volume 78, pages 1031–1040, 1993

Fluorine iron biotite from the Honeycomb Hills rhyolite, Utah: The halogen record of decompression in a silicic magma

W. P. Nash
Department of Geology and Geophysics, University of Utah, Salt Lake City, Utah 84112-1183, U.S.A.

Abstract

Topaz rhyolite of the Honeycomb Hills, Utah, contains Fe-rich biotite with F contents ranging from 2 to 8 wt%. Biotite in the early erupted pyroclastic deposit contains less F on average (~3%) than that in later erupted lavas (~6%), which form the overlying dome. Values of f_{H_2O} in the pyroclastic sequence range from 1050 to 2025 bars, whereas they are less (25–425 bars) in the dome. The ratio of f_{H_2O}/f_{HF} is an order of magnitude higher in the pyroclastic sequence compared with domal lavas. The enrichment of F in biotite in domal lavas, together with lower f_{H_2O}/f_{HF}, is attributed to preferential loss of H_2O over F during slow and essentially isothermal decompression of the magma following the initial explosive phase of the eruption.

Introduction

F-enriched iron biotite is present in rhyolite at the Honeycomb Hills in west-central Utah. The Fe^{2+}-F avoidance rule, which states that F is more readily accommodated in Mg-rich as opposed to Fe-rich members of an isomorphous solid solution series, suggests that these micas should be uncommon; their presence indicates conditions of extremely elevated F activity in a silicic magma. It has been recognized for some time that, in general, F contents of biotite tend to decrease with increasing Fe content. The principle of Fe^{2+}-F avoidance, first put forth by Ramberg (1952) on the basis of Mg-F bonds that are stronger than Fe-F bonds, has been augmented by crystal-field arguments (Rosenberg and Foit, 1977), experiment (Munoz and Ludington, 1974), NMR spectral studies (Sanz and Stone, 1979), and observation (Jacobs and Parry, 1979; Petersen et al., 1982; Valley et al., 1982; Spear, 1984; Munoz, 1984; van Middelaar and Keith, 1990). This paper describes the occurrence and chemical composition of unusual Fe-rich micas whose F and Cl contents record changes in the ratio of H_2O to halogens in a silicic magma during an eruptive cycle.

Host lavas

Rhyolite lava of the Honeycomb Hills, west-central Utah, was erupted 4.7 Ma, forming a dome 1000 m in diameter with a present-day height of 250 m. Domal lavas overlie 12 m of tephra fall deposits. Because the dome is partially eroded, it is possible to sample the rhyolite from the first-erupted pumice to the last-erupted lava in the central conduit. The rhyolites of the Honeycomb Hills are the products of a highly differentiated silicic magma with anomalous concentrations of Li, Be, B, Sn, Y, Rb, and F (Congdon and Nash, 1988, 1991). F contents of >3% have been measured in vitrophyre glass and in melt inclusions in quartz phenocrysts (Gavigan et al., 1989, 1991), and the melt was saturated in F with respect to the minerals fluorite (CaF_2) and fluocerite [$(Ce,La)F_3$]. Phenocrysts consist of quartz, sanidine, oligoclase, biotite, and topaz and range in abundance from 10% in early pumice to 50% in the interior of the dome. Accessory phases occurring as microphenocrysts or inclusions in biotite and topaz include magnetite, fluorite, zircon, thorite, monazite, fluocerite, and the niobates columbite, fergusonite, and ishikawaite. Domal lavas are entirely crystalline and vesicles are extremely uncommon. In terms of their chemical and mineralogical composition, lavas of the Honeycomb Hills resemble rhyolite of Spor Mountain, Utah (Webster et al., 1987; Christiansen et al., 1986), and hypabyssal ongonite in the former Soviet Union (Kovalenko, 1973; Kovalenko et al., 1971, 1977).

The preeruptive magma was compositionally and thermally zoned, as revealed by systematic changes in whole-rock, glass, and mineral compositions related to the sequence of eruption (Congdon and Nash, 1991; Byrd and Nash, 1993). Examples of variation in composition, temperature, and crystal content with eruptive order are shown in Figure 1. Chemical gradients extend upward through the pyroclastic sequence and continue in the dome immediately overlying the tuff to the central conduit. The early erupted magma is more differentiated, as illustrated by elevated concentrations of Rb and reduced amounts of Fe. The distribution of volatile constituents in the preeruptive magma body is more difficult to establish because the components are fugitive and are lost from the system, at least in part, during eruption and crystallization. An understanding of how volatile constituents were distributed in the magma prior to eruption is important to the evaluation of how they were redistributed during eruption. Analyses of melt inclusions in quartz phenocrysts (Gavigan et al., 1989, 1991) revealed gradients in H_2O and F but not Cl in the magma body prior to eruption. F was enriched upward in the preeruptive magma

0003–004X/93/0910–1031$02.00

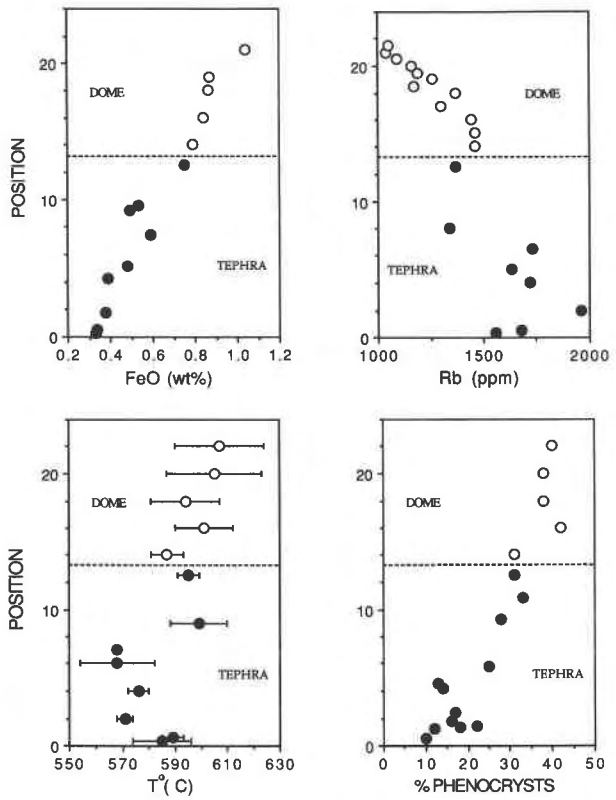

Fig. 1. Examples of chemical, thermal, and physical gradients in the preeruptive magma body of the Honeycomb Hills. Parameters are plotted against stratigraphic position given in meters in the tephra sequence (0–13 m), and in the relative order of eruption in the domal lavas (14–22) (cf. Congdon and Nash, 1991). Temperatures are determined from coexisting plagioclase and alkali feldspar (Fuhrman and Lindsley, 1988); data are from Congdon and Nash (1991). Solid circles are from tephra; open circles are from the overlying dome.

from 2 wt% in the last-erupted material to 3 wt% in the first pumice. H_2O in melt inclusions increased upward in the magma body from 2 wt% in domal lavas to 5 wt% in early erupted pumice. In contrast, Cl showed no significant trend, with concentrations ranging between 0.2 and 0.1%. Similar concentrations of F and Cl were also found in nonvesiculated vitrophyre and, for Cl, in pumice glass.

Analytical methods

Concentrations of major and minor elements in biotite were measured with a Cameca SX-50 electron microprobe. Analytical conditions were 15-keV accelerating voltage, 30-nA beam current, and a beam diameter of 10 μm. Standards used were synthetic fluorphlogopite (F, Mg), natural iron biotite (Al, Si, K, Fe), albite (Na), tugtupite (Cl), diopside (Ca), rutile (Ti), rhodonite (Mn), lepidolite (Rb), and Sn metal. Matrix effects were corrected by a $\phi(\rho Z)$ procedure (Pouchou and Pichoir, 1991). Biotite samples were examined for included accessory phases by backscattered electron imaging. Niobates, monazite, zircon, and thorite were observed. These phases are characterized either by high reflectivity and, for the latter three, by cathodoluminescence, and care was taken to avoid them during analysis. Li was analyzed in two mineral separates by atomic absorption spectroscopy, and Fe^{2+} was determined on sample 32 by titration with ferrous ammonium sulfate, following oxidation of the sample with ammonium metavandate. The H_2O content of biotite sample 32 was determined manometrically on a H extraction line.

Composition of mica

Fluorbiotite occurs as phenocrysts up to 1 mm in diameter, as groundmass crystals, and as occasional megacrysts up to 2 cm in diameter. Biotite contains inclusions of columbite, fergusonite, monazite, zircon, and thorite, and mica is typically included in fluortopaz or surrounds early formed phenocrysts of fluortopaz. Biotite in pumice and vitrophyre is unaltered, whereas biotite from domal felsites is typically oxidized.

Biotite was analyzed from six horizons in the pyroclastic sequence (samples 1, 42, 43, 45, 47, and 48), from a vitrophyric bomb bed at the top of the pyroclastic sequence (samples 10 and 32), and from six felsite samples in the rhyolite dome (samples 20, TH, BH13, 60, 3C, and 1C). Sample 20 is from 1 m above the tephra dome contact; the remainder of the felsites are from the interior of the dome, with 3C near the conduit and 1C within the conduit. Petrographic and chemical descriptions for the host rocks were provided by Congdon and Nash (1991).

Microprobe analyses of biotite and structural formulae are presented in Tables 1 and 2. The two samples (1 and 32) analyzed for Li by atomic absorption both yielded 0.10 wt% Li. The Fe^{2+} determination on sample 32 provides a ratio of $Fe^{2+}/(Fe^{2+} + Fe^{3+})$ of 0.85, consistent with an oxidation state approximately midway between Ni-NiO and Fe_3O_4-Fe_2O_3 (Wones and Eugster, 1965). This compares well with an f_{O_2} of $10^{-17.4}$ bars at 600 °C calculated from the Fe^{3+}/Fe^{2+} ratio of whole-rock sample HH32 (Congdon and Nash, 1991). Lower analytical totals in biotite from the dome are attributed to the effects of posteruption oxidation, which may have converted much of the FeO to Fe_2O_3. The H_2O content of sample 32, measured manometrically, is 1.01 wt%. This is considerably less than the H_2O content calculated from the stoichiometry of the OH site (2.32%).

In terms of major elements, the micas are aluminous, Fe-rich, contain almost no Mg, and have more Rb than Na. Structural formulae reveal the aluminous nature of the micas, which contain up to 85% of the siderophyllite end-member calculated according to the formulation of Gunow et al. (1980; see also Munoz, 1984). High siderophyllite contents are characteristic of biotite from rare-element pegmatites (Černý and Burt, 1984).

The variation in chemical composition of biotite with the order of eruption (stratigraphic position) is illustrated in Figure 2. Biotite from the pyroclastic sequence is usually homogeneous and displays small changes in com-

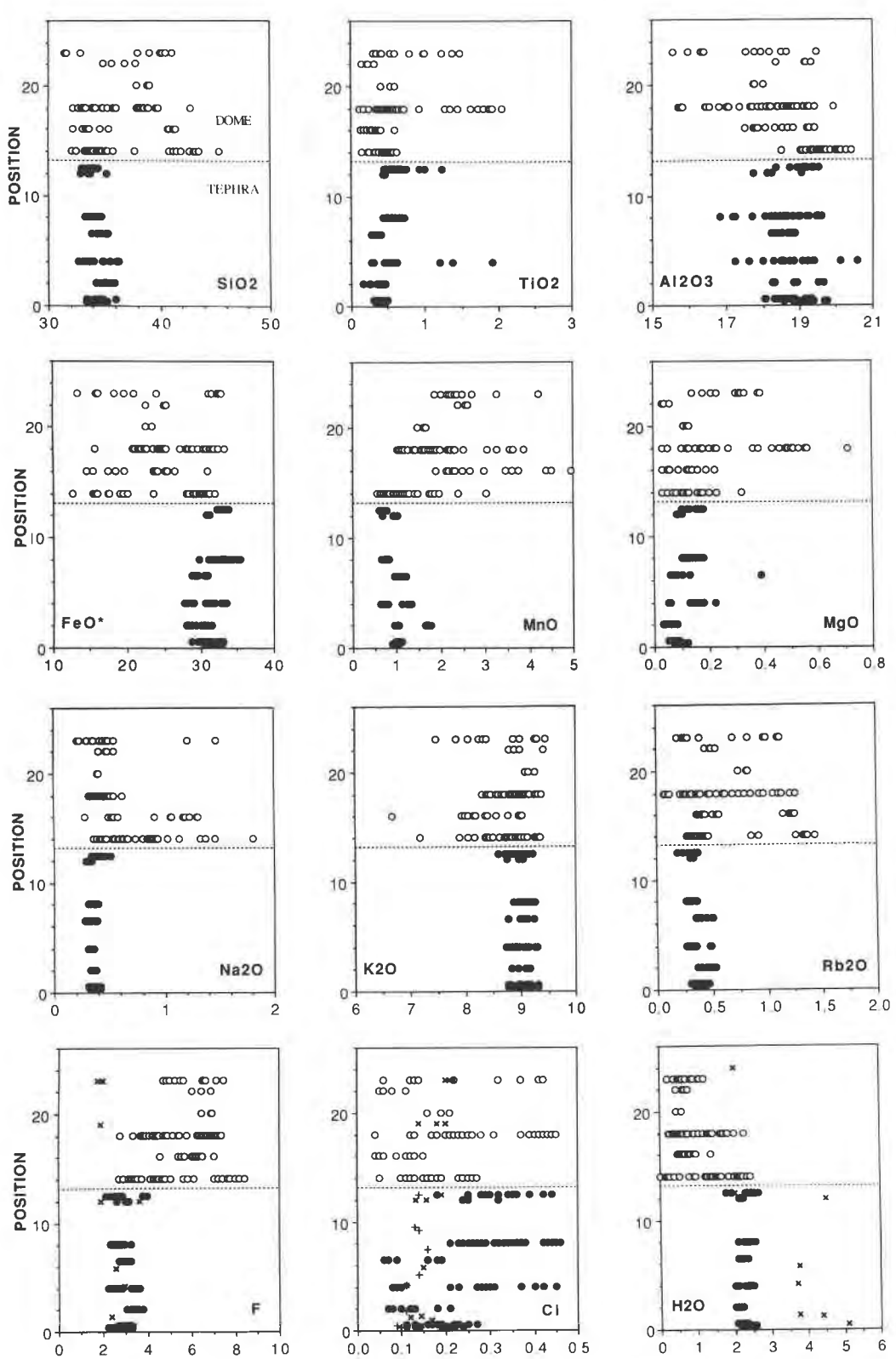

Fig. 2. Compositional variation in biotite and glass (volatiles only) as a function of stratigraphic position. Solid circles = tephra; open circles = dome lavas; × = melt inclusion glass; + = pumice glass.

TABLE 1. Average microprobe analyses of biotite from Honeycomb Hills rhyolite

	Tephra						Vitrophyre	Dome	
	1	42	43	45	47	48	32	20	TH
n	15	17	9	18	9	29	20	34	16
SiO_2	34.3(0.5)	34.4(0.6)	35.1(0.5)	34.0(1.0)	34.7(0.5)	33.8(0.4)	33.8(0.4)	36.2(3.7)	36.0(3.6)
TiO_2	0.42(0.04)	0.43(0.06)	0.35(0.10)	0.57(0.29)	0.34(0.05)	0.59(0.08)	0.68(0.19)	0.47(0.10)	0.34(0.11)
SnO_2	0.06(0.03)	0.08(0.03)	0.09(0.04)	0.08(0.04)	0.07(0.04)	0.04(0.03)	0.05(0.04)	0.06(0.03)	0.09(0.03)
Al_2O_3	19.2(0.3)	18.7(0.4)	19.1(0.6)	18.7(0.7)	18.5(0.2)	18.5(0.7)	19.0(0.2)	19.6(0.4)	18.3(0.7)
Fe_2O_3	—	—	—	—	—	—	8.22	—	—
FeO**	31.9(0.6)	31.0(1.1)	29.7(1.2)	30.7(1.8)	29.8(0.8)	32.5(1.3)	24.7(0.52)	26.3(6.0)	22.6(4.4)
MnO	0.97(0.04)	1.04(0.05)	1.38(0.37)	0.87(0.25)	1.07(0.08)	0.74(0.04)	0.73(0.04)	1.17(0.53)	3.12(0.99)
MgO	0.09(0.02)	0.07(0.01)	0.06(0.02)	0.13(0.05)	0.12(0.10)	0.13(0.02)	0.14(0.02)	0.12(0.06)	0.11(0.05)
CaO	—	—	—	—	—	—	—	0.04(0.06)	0.04(0.05)
Na_2O	0.35(0.03)	0.38(0.03)	0.35(0.02)	0.34(0.02)	0.33(0.03)	0.36(0.02)	0.40(0.02)	0.77(0.34)	0.86(0.36)
K_2O	9.00(0.17)	9.02(0.13)	9.06(0.10)	8.98(0.17)	9.04(0.12)	9.07(0.09)	8.97(0.17)	8.70(0.46)	8.34(0.59)
Rb_2O	0.37(0.03)	0.37(0.04)	0.44(0.05)	0.35(0.08)	0.40(0.06)	0.30(0.02)	0.30(0.04)	0.59(0.41)	0.68(0.38)
F	2.91(0.32)	3.03(0.16)	3.41(0.22)	2.77(0.44)	3.02(0.16)	2.67(0.17)	2.73(0.43)	5.13(1.76)	6.00(0.58)
Cl	0.19(0.04)	0.19(0.05)	0.13(0.04)	0.26(0.12)	0.14(0.05)	0.32(0.07)	0.31(0.06)	0.18(0.06)	0.10(0.03)
H_2O†	2.31(0.14)	2.22(0.07)	2.09(0.09)	2.30(0.15)	2.21(0.07)	2.35(0.08)	1.01(0.04)	1.27(0.77)	0.75(0.23)
Total	102.1	101.0	101.3	99.5	99.8	101.4	101.1	100.5	97.3
−O = F,Cl	1.3	1.3	1.5	1.2	1.3	1.2	1.2	2.2	2.5
Total	100.8	99.7	99.8	98.3	98.5	100.2	99.9	98.3	94.8

* The 2-cm megacryst from topaz horizon (sample TH).
** Fe_{tot} as FeO except for 32, where FeO and Fe_2O_3 were determined.
† H_2O by stoichiometry except for 32, where H_2O was determined manometrically.

position as a function of the order of eruption. In contrast, biotite from the overlying dome displays considerable compositional variation between and within individual samples. The homogeneity and systematic variation in composition of biotite from the tephra indicate that it was in equilibrium with the magma, and it records preeruptive conditions in the uppermost portions of the magma reservoir. Biotite from the most evolved portion of the reservoir, i.e., in the earliest erupted pumice, is relatively enriched by small amounts in Si, Mn, and Rb compared with the last erupted in the pyroclastic sequence (the vitrophyric bomb bed at 12.5 m, sample 32). Similarly, early erupted biotite is slightly poorer in Fe, Mg, Ti, and Cl; Al remains essentially constant with the stratigraphic position. Cl increased with the order of eruption in the pyroclastic sequence; this reflects a twofold increase in Cl content downward in the preeruptive magma reservoir. It is not a consequence of the Mg-Cl avoidance rule (Munoz, 1984), because Mg in biotite also increased slightly as the eruption proceeded. The preci-

TABLE 2. Structural formulae of biotite based on 22 O atoms

	Tephra						Vitro-phyre	Dome						
	1	42	43	45	47	48	32	20	TH	60	BH13	3C	1C	M
Si	5.50	5.58	5.64	5.55	5.65	5.49	5.46	5.78	5.95	5.86	6.22	5.91	5.97	5.82
$^{[4]}Al$	2.50	2.42	2.36	2.45	2.35	2.51	2.54	2.54	2.05	2.14	1.78	2.09	2.03	2.18
	8.00	8.00	8.00	8.00	8.00	8.00	8.00	8.00	8.00	8.00	8.00	8.00	8.00	8.00
$^{[6]}Al$	1.14	1.15	1.25	1.14	1.22	1.03	1.08	1.48	1.52	1.31	1.60	1.56	1.36	1.46
Ti	0.05	0.05	0.04	0.08	0.04	0.07	0.08	0.06	0.04	0.09	0.06	0.03	0.10	0.02
Fe	4.28	4.20	3.99	4.18	4.07	4.41	4.34	3.54	3.12	3.58	3.06	3.24	3.32	3.57
Mn	0.13	0.14	0.18	0.12	0.14	0.10	0.10	0.16	0.43	0.26	0.22	0.35	0.33	0.24
Mg	0.02	0.02	0.01	0.03	0.03	0.03	0.03	0.03	0.03	0.06	0.03	0.01	0.07	0.00
Ca	0.00	0.00	0.00	0.00	0.00	0.00	0.00	0.01	0.01	0.00	0.00	0.00	0.00	0.00
	5.63	5.57	5.50	5.56	5.51	5.65	5.64	5.26	5.15	5.30	4.98	5.19	5.20	5.39
Na	0.11	0.12	0.11	0.11	0.10	0.11	0.13	0.28	0.28	0.14	0.13	0.15	0.15	0.12
K	1.84	1.86	1.86	1.87	1.88	1.88	1.85	1.76	1.76	1.83	1.88	1.87	1.82	1.88
Rb	0.04	0.04	0.05	0.04	0.04	0.03	0.03	0.06	0.07	0.06	0.08	0.05	0.06	0.05
	1.99	2.02	2.02	2.02	2.02	2.02	2.01	2.08	2.12	2.03	2.09	2.07	2.05	2.05
F	1.48	1.55	1.73	1.43	1.56	1.37	1.39	2.59	3.14	2.87	3.43	3.31	3.15	2.25
Cl	0.05	0.05	0.03	0.07	0.04	0.09	0.09	0.05	0.03	0.07	0.05	0.02	0.07	0.02
OH	(2.47)	(2.40)	(2.23)	(2.50)	(2.40)	(2.54)	(2.52)	1.36	(0.83)	(1.05)	(0.52)	(0.67)	(0.78)	(1.73)
	4.00	4.00	4.00	4.00	4.00	4.00	4.00	4.00	4.00	4.00	4.00	4.00	4.00	4.00
X_F*	0.37	0.39	0.43	0.36	0.39	0.34	0.35	0.65	0.79	0.72	0.86	0.83	0.79	0.56
X_{Phl}**	0.00	0.00	0.00	0.01	0.01	0.01	0.01	0.01	0.01	0.01	0.01	0.00	0.01	0.00
X_{Ann}**	0.15	0.18	0.18	0.17	0.19	0.17	0.15	0.18	0.24	0.25	0.33	0.21	0.29	0.20
X_{Sid}**	0.85	0.82	0.82	0.82	0.80	0.82	0.84	0.81	0.75	0.74	0.66	0.79	0.70	0.80

* Atom fraction F in OH site.
** Mole fraction end-members (after Munoz, 1984).

TABLE 1.—*Continued*

Dome				
60	BH13	3C	1C	M*
33	3	4	11	9
36.2(2.7)	38.6(0.6)	36.3(1.3)	36.0(4.4)	35.9(0.8)
0.77(0.54)	0.52(0.10)	0.23(0.07)	0.83(0.42)	0.14(0.03)
0.04(0.04)	0.04(0.02)	0.07(0.02)	0.06(0.04)	0.12(0.03)
18.1(1.1)	17.8(0.2)	19.0(0.4)	17.4(1.3)	19.1(0.5)
—	—	—	—	—
26.4(4.2)	22.7(0.51)	23.8(1.6)	24.0(7.9)	26.3(1.5)
1.90(0.68)	1.58(0.10)	2.54(0.10)	2.35(0.37)	1.78(0.09)
0.24(0.17)	0.13(0.01)	0.05(0.02)	0.30(0.07)	—
—	—	—	0.03(0.01)	—
0.43(0.06)	0.41(0.00)	0.47(0.05)	0.48(0.35)	0.39(0.02)
8.86(0.26)	9.15(0.09)	9.01(0.27)	8.63(0.68)	9.09(0.19)
0.54(0.37)	0.78(0.05)	0.49(0.04)	0.62(0.39)	0.44(0.02)
5.61(1.34)	6.73(0.25)	6.42(0.37)	6.01(0.97)	4.38(0.68)
0.27(0.11)	0.19(0.02)	0.07(0.03)	0.24(0.14)	0.07(0.01)
0.97(0.57)	0.49(0.09)	0.62(0.78)	0.71(0.31)	1.60(0.35)
100.3	99.2	99.0	97.7	99.2
2.4	2.9	2.7	2.6	1.8
97.9	96.3	96.3	95.1	97.4

sion of the Sn analyses is poor, and they have not been plotted; however it is evident that Sn decreases slightly in biotite from the bottom to the top of the pyroclastic sequence (Table 1). The covariance of elements in biotite is illustrated in Figure 3, where concentrations are plotted against F content. There is a positive correlation of Si, Mn, Na, and Rb with F. Mg, Ti, and K show little correlation with F, whereas Fe shows a pronounced negative correlation with F, a reflection of the Fe-F avoidance principle. The high increase in Rb may indicate a strong preference for fluorine micas, analogous to the behavior of Li.

Biotite from the dome is more varied in composition and displays considerable heterogeneity, even within a single hand sample. In contrast to biotite from the underlying tuff, domal biotite has increased amounts of Si, Mn, Na, Rb, and F, and lesser amounts of Fe (Fig. 2). Because the lavas of the dome are chemically similar to the underlying pumices, I believe that the significant compositional differences between biotite from the two units are due to the reaction of biotite in the dome-forming magma to changing physical conditions, including the composition of the residual melt, the evolution of a fluid phase, a decrease in pressure, and the accompanying rise in the temperature of the solidus.

HALOGENS AND H_2O

Micas from the Honeycomb Hills display a bimodal distribution of F contents (Fig. 2). Biotite from the pyroclastic sequence has approximately half of the OH site filled with F, whereas biotite from the passively erupted domal lavas have the OH site occupied from 50 up to 95% by F. This significant difference in F content is interpreted to be due to a change in the f_{H_2O}/f_{HF} ratio in the magma between the time immediately prior to explosive venting of the magma chamber and the subsequent eruption and crystallization of the domal lavas (see below). Elevated F concentrations in biotite from dome felsites are not attributed to postmagmatic processes. Hildreth (1977) concluded that postmagmatic exchange of volatiles in the Bishop Tuff resulted in lower F contents in biotite, whose present compositions could not be in equilibrium with magmatic fluorapatite. Keith and Shanks (1988) observed that siderophyllite in lavas is often oxidized and contains less F than biotite from associated ash-flow tuffs in the Pine Grove, Utah, system; they attributed the reduction in F, as well as Cl, to postmagmatic exchange. Hydrothermal alteration of biotite results in a significant increase in Mg content (Jacobs and Parry, 1979). There is no evidence of hydrothermal alteration at the Honeycomb Hills, and other minerals susceptible to hydrothermal alteration, such as feldspar, show no evidence of reaction.

As a basis for comparison with biotite, F, Cl, and H_2O concentrations in pumice glass and melt inclusions in coexisting quartz phenocrysts are illustrated in Figure 2. The F content of biotite in pumices are essentially equal to the F content of the coexisting glass, whereas domal biotite has F contents considerably in excess of the glass. Cl concentrations in biotite of the tephra typically equal or exceed the Cl concentration in coexisting glass. Biotite from the dome has a wide range in Cl contents, although a great percentage has less Cl than in the preeruptive melt. At the Honeycomb Hills, the calculated H_2O contents of biotite are approximately half the H_2O concentration in the melt determined from melt inclusions in quartz phenocrysts.

The experimental studies of Munoz and Ludington (1974), Gunow et al. (1980), and Munoz and Swenson (1981) established functions for fugacity ratios as follows:

$$\log(f_{H_2O}/f_{HF}) = 2100/T + 1.523X_{Phl} + 0.416X_{Ann} + 0.200X_{Sid} - \log(X_F/X_{OH}) \quad (1)$$

$$\log(f_{H_2O}/f_{HCl}) = 5151/T - 5.01 - 1.93X_{Phl} - \log(X_{Cl}/X_{OH}) \quad (2)$$

$$\log(f_{HCl}/f_{HF}) = -3051/T + 5.01 + 3.45X_{Phl} + 0.42X_{Ann} + 0.20X_{Sid} - \log(X_F/X_{Cl}) \quad (3)$$

where $X_{Phl} = X_{Mg}/^{[6]}X$, $X_{Sid} = [(3 - Si/Al)/1.75](1 - X_{Phl})$, and $X_{Ann} = 1 - (X_{Phl} - X_{Sid})$ (Munoz, 1984). $X_{OH} = 1 - (X_F + X_{Cl})$ and represents a maximum value for X_{OH} because the amount of O^{2-} is not established. The presence of O^{2-} would not change X_F or X_{Cl} but would reduce X_{OH} as calculated.

Fugacity ratios, calculated over the temperature gradient 575–605 °C (Fig. 1), are presented in Table 3 and illustrated as a function of the sequence of eruption in Figure 4. The ratio f_{H_2O}/f_{HF} has average and constant values of approximately 800 in the tephra and 110 in

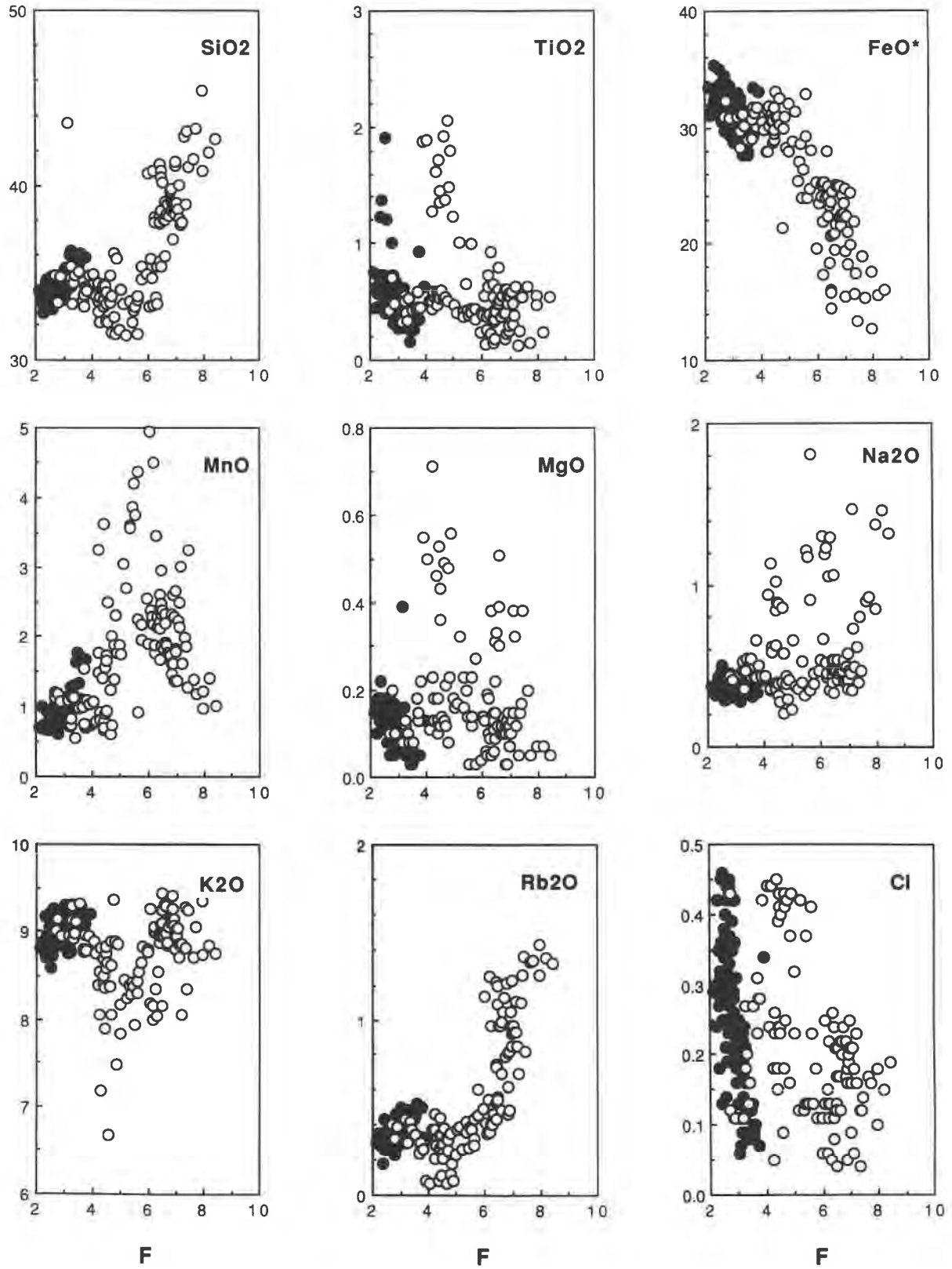

Fig. 3. Compositional variation in biotite as a function of F content. Symbols are as in Fig. 1.

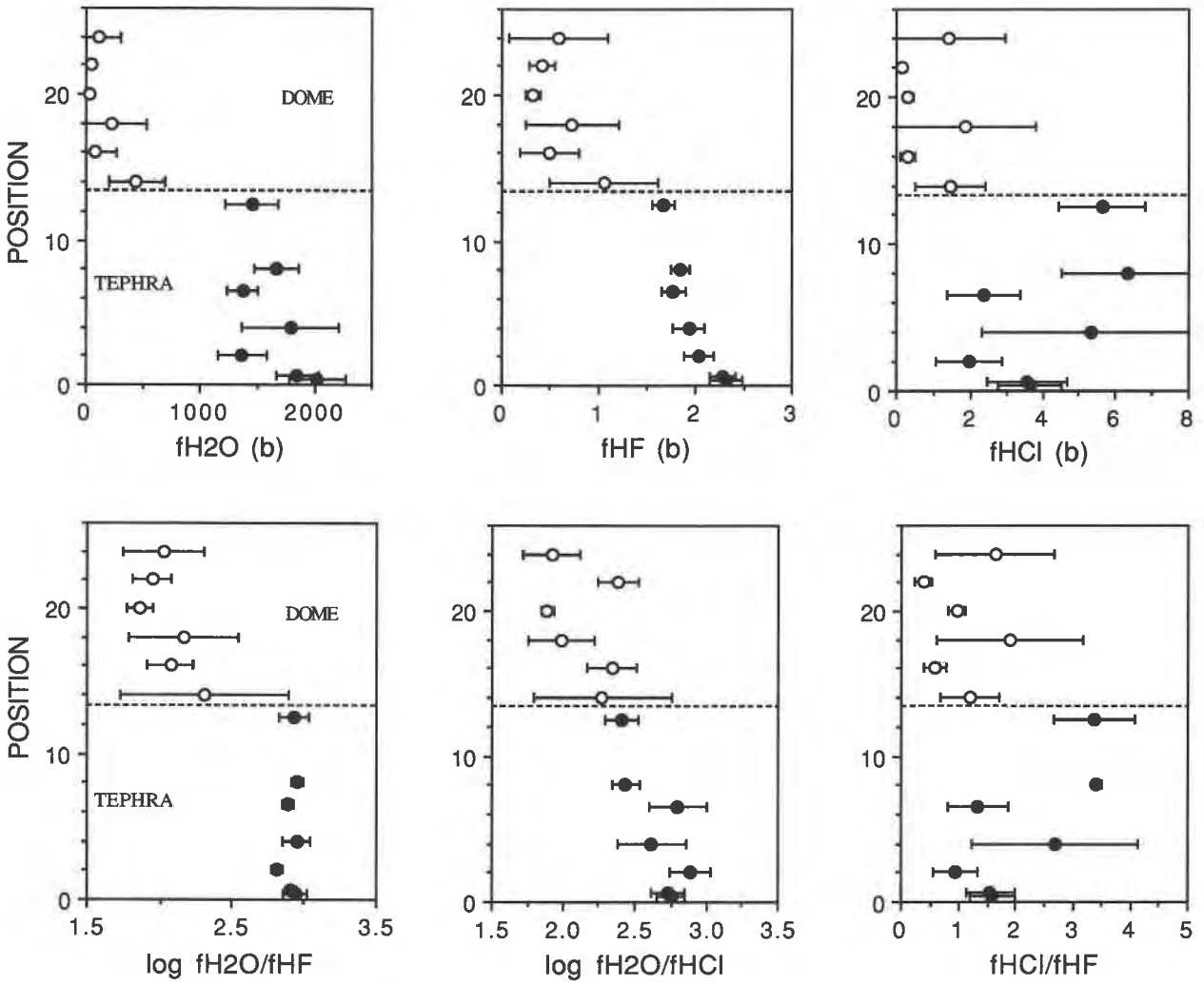

Fig. 4. Fugacities and fugacity ratios in the fluid phase calculated from biotite compositions plotted against stratigraphic position. Bars indicate the range in calculated values resulting from the variation in chemical composition of biotite, as illustrated in Fig. 2. Symbols are as in Fig. 1.

TABLE 3. Position, temperature, and fugacity parameters for Honeycomb Hills rhyolite

Sample	Position*	T (°C)**	f_{H_2O}†	f_{HF}†	f_{HCl}†	$\log(f_{H_2O}/f_{HF})$	$\log(f_{H_2O}/f_{HCl})$	f_{HCl}/f_{HF}
				Tephra				
1	0.4	575	2025 ± 250	2.3 ± 0.2	3.7 ± 0.9	2.94 ± 0.08	2.75 ± 0.11	1.58 ± 0.40
42	0.6	575	1050 ± 180	2.3 ± 0.1	3.6 ± 1.1	2.91 ± 0.03	2.73 ± 0.12	1.55 ± 0.43
43	2	577	1370 ± 220	2.0 ± 0.2	2.0 ± 0.9	2.82 ± 0.04	2.88 ± 0.14	0.94 ± 0.38
45	4	580	1790 ± 430	1.9 ± 0.2	5.3 ± 3.0	2.95 ± 0.10	2.62 ± 0.25	2.61 ± 1.47
47	6.5	584	1370 ± 130	1.8 ± 0.1	2.4 ± 1.0	2.89 ± 0.04	2.80 ± 0.20	1.33 ± 0.53
48	8	587	1670 ± 190	1.8 ± 0.1	6.4 ± 1.8	2.96 ± 0.04	2.44 ± 0.10	3.41 ± 0.86
32	12.5	592	1450 ± 230	1.7 ± 0.1	5.6 ± 1.2	2.93 ± 0.10	2.41 ± 0.11	3.37 ± 0.70
				Dome				
20	14	594	426 ± 365	1.1 ± 0.6	1.5 ± 1.0	2.31 ± 0.58	2.27 ± 0.48	1.18 ± 0.51
TH	16	597	76 ± 92	0.5 ± 0.3	0.3 ± 0.2	2.08 ± 0.16	2.34 ± 0.17	0.58 ± 0.18
60	18	600	231 ± 269	0.7 ± 0.5	1.9 ± 1.9	2.17 ± 0.38	1.99 ± 0.23	1.90 ± 1.28
BH13	20	600	25 ± 11	0.3 ± 0.1	0.3 ± 0.1	1.87 ± 0.09	1.89 ± 0.05	0.95 ± 0.14
3C	22	603	41 ± 22	0.4 ± 0.1	0.2 ± 0.1	1.95 ± 0.13	2.39 ± 0.14	0.38 ± 0.14
1C	24	605	105 ± 117	0.6 ± 0.5	1.4 ± 1.6	2.03 ± 0.28	1.92 ± 0.20	1.63 ± 1.04

* Positions 0.4–12.5 represent elevation in meters above base of the tephra sequence. Positions 14–24 represent relative sequence of eruption of dome lavas from the base of the dome (14) to the central conduit (24).

** Temperature used in calculations derived from a linear fit to the data illustrated in Fig. 1.

† Ranges in values represent 1 sd from the mean (see text).

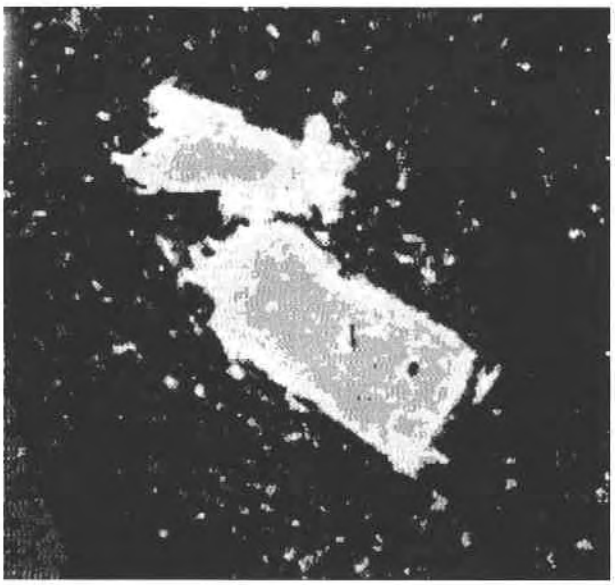

Fig. 5. X-ray intensity map of F distribution in biotite phenocryst from sample 20, located immediately above the tephra dome contact (position 14, Fig. 2). The image records a rim enriched in F surrounding a core whose F content is similar to those of biotite in the underlying tephra.

domal lavas, representing a decrease of almost an order of magnitude between the two phases of the eruption. The ratio in the tephra is similar to that calculated for micas at 450 °C in the Henderson molybdenum deposit (Gunow et al., 1980), whereas the values for the domal lavas are, to my knowledge, the most F-rich ratios yet reported.

The f_{H_2O}/f_{HCl} ratio declines through the eruptive sequence from average values of 600 in the first-erupted pumice to 200 in the tuff-capping vitrophyre and 100 in the interior of the dome. The declining fugacity ratio in the preeruptive magma recorded in the tephra sequence continues in the dome but with greater variation in the Cl content of biotite from the same host rock. The ratio f_{HCl}/f_{HF} increases in general from near unity in early erupted pumices to about four in the upper pyroclastic sequence, whereas the trend is reversed in the dome.

Absolute fugacities of the volatile species can be calculated from the experimental biotite equilibria of Wones and Eugster (1965). For the calculations presented here, I have adopted the equilibrium constant advocated by Hildreth (1977):

$$\log f_{H_2O} = 8673/T + 2.46 + \tfrac{1}{2} \log f_{O_2} + \log a_{Ann} - \log a_{San} - \log a_{Mt}. \quad (4)$$

The activity of annite assumes an ideal mixing model:

$$a_{Ann} = ({}^{[12]}X_K)({}^{[6]}X_{Fe})^3(X_{OH})^2. \quad (5)$$

The activity of sanidine ($Or_{0.667}Ab_{0.030}An_{0.003}$) is calculated to be 0.75, using the composition-activity relationship of Fuhrman and Lindsley (1988). Reconnaissance analyses of magnetite indicate negligible Ti, and the activity of magnetite is taken to be 1.0. At an f_{O_2} of $10^{-17.4}$ bars (Congdon and Nash, 1991) values of f_{H_2O} range from 2000–1400 bars through the pyroclastic sequence, dropping to 400–25 bars in domal lavas (Table 3, Fig. 4). Values of f_{HF} decline regularly from 2.3 bars in early erupted pumices to 1.7 bars in vitrophyre, and continue to decrease in felsite from 1 to 0.5 bars. Values of f_{Cl} increase through the pyroclastic sequence and decline abruptly in domal lavas.

The uncertainties in fugacities reported in Table 3 and illustrated in Figure 4 result from the range in composition of biotite within individual samples (cf. Table 1, Fig. 2). Ranges in fugacities represent 1 sd from the mean of results calculated for each individual biotite analysis in a given sample. These ranges do not constrain accuracies of the computed fugacities. Further, it should be noted that X_{OH} is determined in the OH site from stoichiometry, not by direct analysis. As observed by Munoz (1984), it is a common occurrence to have deficiencies in the OH site, as observed in sample 32, for which H_2O was determined. Accordingly, care should be exercised in interpreting these results. The principal observation is that they represent significant relative differences between the composition of the fluid phase before and after the explosive phase of the eruption.

In interpreting these results, it is important to recognize that the calculations are for equilibrium assemblages, whereas it is evident from the wide range of biotite compositions in individual samples of domal lavas that equilibrium was not universally attained. In contrast, biotite from tephra is homogeneous, and the assumption of equilibrium appears to be reasonable. Accordingly, fugacities and fugacity ratios calculated for the dome should be regarded as approximate and as trends in volatile activities recorded by the attempted reequilibration of biotite with an evolving fluid phase. Evidence of partial reaction is provided by biotite from near the base of the dome (sample 20). This sample is representative of the first lavas to be extruded after the explosive phase of the eruption. Biotite in sample 20 possesses cores with compositions similar to those in the tephra and rims similar to biotite from the interior of the dome (Fig. 5).

Discussion

One of the ways silicic magmas change the concentration of their volatiles is in response to decompression. Volatiles are lost to the surrounding environment when fluid pressures in the magma are in excess of the lithostatic load during ascent. However, in an eruption, decompression of the magma may occur in very different time scales. At the Honeycomb Hills, there were two stages of degassing of the magma. The first was catastrophic vesiculation, producing fragmentation of the magma in the uppermost levels of the reservoir and its conduit, which resulted in eruption and deposition of the pyroclastic sequence. The second degassing accompanied the passive

ascent of the magma volume that ultimately gave rise to the nonvesicular domal lavas.

The various volatile components of a magma partition themselves differently during the evolution of a discrete fluid phase. H_2O, partitioning strongly into the fluid phase, is the dominant component. F, on the other hand, favors the silicate melt by about 3:1 (Dingwell et al., 1985; Webster, 1990; Webster and Holloway, 1990). In topaz rhyolites, Cl has a vapor-melt partition coefficient between 2 and 10 (Webster and Holloway, 1990). Accordingly, during the evolution of a fluid phase, the fugacity ratios f_{H_2O}/f_{HF} and f_{HCl}/f_{HF} should decrease. Biotite in the pyroclastic sequence records fugacity ratios prior to eruption, and because of the instantaneous nature of the eruption and rapid cooling, these biotite samples failed to reequilibrate with the evolving magmatic fluid phase. Conversely, biotite in the unfragmented magma had sufficient time to react as the degassing magma rose passively to the surface over a period of weeks or months, thus recording the preferential loss of H_2O and Cl over F in the fluid phase. Biotite near the base of the dome, which was erupted early in the formation of the lava dome, evidently did not have sufficient time to react completely with the evolving fluid phase (Fig. 5).

The conditions in the magma body prior to and after degassing are evident in the fugacity ratios illustrated in Figure 4. Ratios of f_{H_2O}/f_{HF} remain nearly constant in the pyroclastic sequence, reflecting the upward enrichment in both H_2O and F in the preeruptive magma reservoir. The precipitous decline in this ratio in the felsites of the dome is due to the preferential loss of H_2O and is reflected in the attempted reequilibration of biotite with the changing composition of the more F-enriched fluid phase. Declining f_{H_2O}/f_{HCl} ratios in the pyroclastic sequence are a reflection of the decrease in H_2O and the little change in Cl with depth in the preeruptive magma reservoir. The nearly constant ratios in the dome indicate that, during passive degassing, Cl activity declined in the melt in a manner proportional to H_2O as both were partitioned preferentially into the fluid phase. The increase in the f_{HCl}/f_{HF} ratio in the pyroclastic sequence is due to the enrichment in F relative to Cl in the upper portion of the magma body. The decline in this ratio in the dome records the loss of Cl to the fluid phase during passive degassing. The data on absolute fugacity illustrate that values of f_F were highest in the upper reaches of the magma reservoir. The drop in f_{H_2O}/f_{HF} and f_{HCl}/f_{HF} ratios in the domal lavas is a consequence of dehydration and dechlorination of the magma upon ascent, following the explosive phase of the eruption.

In the past several years, differing views have been expressed about the mechanisms of nonexplosive eruption of silicic magmas. In one model, silicic magma is erupted nonexplosively as a permeable foam that forms rapidly in the subsurface and subsequently collapses during extrusion (Eichelberger et al., 1986; Westrich et al., 1988; Eichelberger, 1989). The essence of this interpretation is that the magma loses all of its volatiles upon ascent. Fink et al. (1992) argued that some magmas may lose volatiles at depth, but they also continue to vesiculate during surface flowage. Both models are designed to accommodate the transition from explosive to nonexplosive eruption, even if strong gradients in the H_2O content are not present in the preeruptive magma body. Although the data presented here do not argue for one or the other of these models, from the evidence at the Honeycomb Hills, I conclude that the eruptive behavior, and especially the transition from explosive to effusive behavior, is controlled primarily by gradients in the volatile and crystal content in the preeruptive magma body. Recent studies of melt inclusions demonstrate that gradients in H_2O are common in high-silica magma bodies (Anderson et al., 1989; Gavigan et al., 1989, 1991; Hervig et al., 1989; Dunbar and Hervig, 1992a, 1992b). Decreasing H_2O content with depth, together with increasing crystallinity, produce a viscosity gradient that ultimately inhibits explosive evacuation of the magma reservoir (Congdon and Nash, 1991). The rise of the magma is slowed, and, as a consequence, volatile loss becomes more gradual. The complete crystallinity of the domal lavas indicates that volatile loss was not so rapid as to cause significant undercooling of the ascending magma. However, it is important to understand that the transition from explosive to nonexplosive behavior is not simply the consequence of an H_2O gradient in the preeruptive magma body. In that conceptual model, the passive extrusion of a dome results from ascent of a volume of magma whose initial H_2O content was low. Evidence from the Honeycomb Hills indicates that the magma volume forming the dome had a higher initial H_2O content, and H_2O continued to be lost from the system upon ascent and prior to eruption. The concentration of F in the residual melt facilitated the passive eruption of a cool, H_2O-poor, and crystal-rich silicic magma.

Acknowledgments

Financial support was provided by NSF grants EAR-86-18101 and EAR-87-20627. I would like to thank Erich Petersen for helpful discussions about biotite stoichiometry and a review of the manuscript. Subsequent reviews by Jim Luhr and Jim Webster tempered my views and materially aided the presentation. They are, however, absolved of any responsibility for the conclusions of this paper.

References cited

Anderson, A.T., Newman, S., Williams, S., Druitt, T., Skirius, E., and Stolper, E. (1989) H_2O, CO_2, Cl and gas in the Plinian and ash-flow Bishop rhyolite. Geology, 17, 221–225.

Byrd, B.J., and Nash, W.P. (1993) Eruption of rhyolite at the Honeycomb Hills, Utah: Cyclical tapping of a zoned silicic magma body. Journal of Geophysical Research, 96, in press.

Černý, P., and Burt, D.M. (1984) Paragenesis, crystallochemical characteristics, and chemical evolution of micas in granitic pegmatites. In Mineralogical Society of America Reviews in Mineralogy, 13, 257–298.

Christiansen, E.H., Sheridan, M.F., and Burt, D.M. (1986) The geology and geochemistry of Cenozoic topaz rhyolites from the western United States. Geological Society of America Special Paper, 205, 81 p.

Congdon, R.D., and Nash, W.P. (1988) High fluorine rhyolite: An eruptive pegmatite magma at the Honeycomb Hills, Utah. Geology, 16, 1018–1021.

——— (1991) Eruption of pegmatite magma: Rhyolite of the Honeycomb Hills. American Mineralogist, 76, 1261–1278.

Dingwell, D.G., Scarfe, C.M., and Cronin, D.J. (1985) The effects of fluorine on viscosities in the system Na_2O-Al_2O_3-SiO_2: Implications for phonolites, trachytes and rhyolites. American Mineralogist, 70, 80–87.

Dunbar, N.W., and Hervig, R.L. (1992a) Petrogenesis and volatile stratigraphy of the Bishop Tuff: Evidence from melt inclusion analysis. Journal of Geophysical Research, 97, 15129–15150.

——— (1992b) Volatile and trace element composition of melt inclusions from the lower Bandelier Tuff: Implications for magma chamber processes and eruptive style. Journal of Geophysical Research, 97, 15151–15170.

Eichelberger, J.C. (1989) Are extrusive rhyolites produced from permeable foam eruptions? Reply. Bulletin Volcanology, 51, 72–75.

Eichelberger, J.C., Carrigan, C.R., Westrich, H.R., and Price, R.H. (1986) Non-explosive silicic volcanism. Nature, 323, 598–602.

Fink, J.H., Anderson, S.W., and Manley, C.R. (1992) Textural constraints on effusive silicic volcanism: Beyond the permeable foam model. Journal of Geophysical Research, 97, 9073–9083.

Fuhrman, M.L., and Lindsley, D.H. (1988) Ternary-feldspar modeling and thermometry. American Mineralogist, 73, 201–215.

Gavigan, T.H., Nash, W.P., and Webster, J.D. (1989) Pre-eruptive gradients in silicic magma as recorded by melt inclusions (abs.). Eos, 70, 1417.

——— (1991) Volatile content of the silicic magma chamber of the Honeycomb Hills, Utah: Complications associated with melt inclusion entrapment and redistribution. Geological Society of America Abstracts with Programs, 23 (5), A442.

Gunow, A.J., Ludington, S., and Munoz, J.L. (1980) Fluorine in micas from the Henderson molybdenite deposit, Colorado. Economic Geology, 75, 1127–1137.

Hervig, R.L., Dunbar, N.W., Westrich, H.R., and Kyle, P.R. (1989) Pre-eruptive water content of rhyolitic magmas as determined by ion microprobe analyses of melt inclusions in phenocrysts. Journal of Volcanology and Geothermal Research, 36, 293–302.

Hildreth, E.W. (1977) The magma chamber of the Bishop Tuff: Gradients in temperature, pressure and composition, 328 p. Ph.D. thesis, University of California, Berkeley, California.

Jacobs, D.C., and Parry, W.T. (1979) Geochemistry of biotite in the Santa Rita porphyry copper deposit, New Mexico. Economic Geology, 74, 860–887.

Keith, J.D., and Shanks, W.C., III (1988) Chemical evolution and volatile fugacities of the Pine Grove porphyry molybdenum and ash-flow tuff system, southwestern Utah. In R.P. Taylor and D.F. Strong, Eds., Recent advances in the geology of granite-related mineral deposits. Canadian Institute of Mining and Metallurgy, Special Volume, 39, 402–423.

Kovalenko, V.I. (1973) Distribution of fluorine in a topaz-bearing quartz keratophyre dike (ongonite) and mobility of fluorine in quartz melts. Geochemistry International, 10, 41–49.

Kovalenko, V.I., Kuz'min, M.I., Antipin, V.S., and Petrov, L.L. (1971) Topaz-bearing quartz keratophyre dike (ongonite), a new variety of subvolcanic igneous vein rock. Doklady Akademie Nauk SSSR, Earth Sciences Section, 199, 132–135.

Kovalenko, V.I., Antipin, V.S., Konusova, V.V., Smirnova, Ye. V., Petrov, L.L., Vladykin, N.V., Kuznetsova, A.I., Kostukova, YeS., and Pisarskaya, V.A. (1977) Partition coefficients of fluorine, niobium, tantalum, lanthanum, ytterbium, yttrium, tin and tungsten in ongonite. Doklady Akademie Nauk SSSR, Earth Sciences Section 233, 203–205.

Munoz, J.L. (1984) F-OH and Cl-OH exchange in micas with applications to hydrothermal ore deposits. In Mineralogical Society of America Reviews in Mineralogy, 13, 469–494.

Munoz, J.L., and Ludington, S.D. (1974) Fluoride hydroxyl exchange in biotite. American Journal of Science, 274, 396–413.

Munoz, J.L., and Swenson, A. (1981) Chloride-hydroxyl exchange in biotite and estimation of relative HCl/HF activities in hydrothermal fluids. Economic Geology, 76, 2212–2221.

Petersen, E.U., Essene, E.J., Peacor, D.R., and Valley, J.W. (1982) Fluorine end-member micas and amphiboles. American Mineralogist, 67, 538–544.

Pouchou, J.-L., and Pichoir, F. (1991) Quantitative analysis of homogeneous or stratified microvolumes applying the model "PAP". In K.F.J. Heinrich and D.E. Newbury, Eds., Electron probe quantitation, p. 31–75. Plenum, New York.

Ramberg, H. (1952) Chemical bonds and the distribution of cations in silicates. Journal of Geology, 60, 331–355.

Rosenberg, P.E., and Foit, F.F., Jr. (1977) Fe^{2+}-F avoidance in silicates. Geochimica et Cosmochimica Acta, 41, 345–346.

Sanz, J., and Stone, W.E. (1979) NMR study of micas. II. Distribution of Fe^{2+}, F^-, and OH^- in the octahedral sheet of phlogopites. American Mineralogist, 64, 119–126.

Spear, J.A. (1984) Micas in igneous rocks. In Mineralogical Society of America Reviews in Mineralogy, 13, 299–356.

Valley, J.W., Petersen, E.U., Essene, E.J., and Bowman, J.R. (1982) Fluorphlogopite and fluortremolite in Adirondack marbles and calculated C-O-H-F fluid composition. American Mineralogist, 67, 545–557.

van Middelaar, W.T., and Keith, J.D. (1990) Mica chemistry as an indicator of oxygen and halogen fugacities in the CanTung and other W-related granitoids in the North American Cordillera. In H.J. Stein and J.L. Hannah, Eds., Ore-bearing granite systems: Petrogenesis and mineralizing processes. Geological Society of America Special Paper, 246, 205–220.

Webster, J.D. (1990) Partitioning of F between H_2O and CO_2 fluids and topaz rhyolite melt. Contributions to Mineralogy and Petrology, 104, 424–438.

Webster, J.D., and Holloway, J.R. (1990) Partitioning of F and Cl between magmatic hydrothermal fluids and highly evolved granitic magmas. In H.J. Stein and J.L. Hannah, Eds., Ore-bearing granite systems: Petrogenesis and mineralizing processes. Geological Society of America Special Paper, 246, 21–34.

Webster, J.D., Holloway, J.R., and Hervig, R.L. (1987) Phase equilibria of a Be, U and F-enriched vitrophyre from Spor Mountain, Utah. Geochimica et Cosmochimica Acta, 51, 389–402.

Westrich, H.R., Stockman, H.W., and Eichelberger, J.C. (1988) Degassing of rhyolite magma during ascent and emplacement. Journal of Geophysical Research, 93, 6503–6511.

Wones, D.R., and Eugster, H.P. (1965) Stability of biotite: Experiment, theory and application. American Mineralogist, 50, 1228–1272.

Manuscript received January 27, 1993
Manuscript accepted May 25, 1993